Journal of the Korean Astronomical Society
50: 179 ∼ 184, 2017 December

https://doi.org/10.5303/JKAS.2017.50.6.179
pISSN: 1225-4614 · eISSN: 2288-890X
http://jkas.kas.org

An Inversion Method for Deriving Physical Properties of a Subsurface Magnetic Field from Surface Magnetic Field Evolution
I. Application to Simulated Data

Tetsuya Magara[1]

[1]Department of Astronomy and Space Science, School of Space Research, Kyung Hee University, 1732 Deogyeong-daero, Giheung-gu, Yongin, Gyeonggi 17104, Korea; magara@khu.ac.kr

Received October 28, 2017; accepted November 18, 2017

Abstract: We present a new method for solving an inverse problem of flux emergence which transports subsurface magnetic flux from an inaccessible interior to the surface where magnetic structures may be observed to form, such as solar active regions. To make a quantitative evaluation of magnetic structures having various characteristics, we derive physical properties of subsurface magnetic field that characterize those structures formed through flux emergence. The derivation is performed by inversion from an evolutionary relation between two observables obtained at the surface, emerged magnetic flux and injected magnetic helicity, the former of which provides scale information while the latter represents the configuration of magnetic field.

Key words: Sun: active regions — Sun: solar magnetism — magnetohydrodynamics — methods: inversion

1. Introduction

We consider magnetic fields rising via magnetic buoyancy (Parker 1955) through a gravitationally bound region filled with a dense plasma. The region is divided into an interior and surface, the latter behaving like a nearly impermeable boundary toward radiative flux, so it is difficult to directly observe subsurface magnetic field in electromagnetic waves. On the other hand, because of its divergence-free nature, magnetic flux is continuous across the surface. Thus physical properties of subsurface magnetic field determine the characteristics of magnetic structures formed on the surface, such as solar active regions producing flares and/or coronal mass ejections (Low 1996; Priest & Forbes 2002; Kliem & Török 2006; Shibata & Magara 2011). A key question is therefore how physical properties of subsurface magnetic field may be derived from observations of surface magnetic field.

The subsurface magnetic field surrounded by a convecting hot and dense plasma is suggested to have the shape of a thin magnetic flux tube with some twist (Moreno-Insertis & Emonet 1996; Fan 2009). To derive physical properties of the subsurface magnetic field, we construct a model for the emergence of a cylindrical flux tube, as illustrated in Figure 1a. Here we use the Cartesian coordinates (X, Y, Z), in which the Y- and Z-axes determine the axial direction of flux tube and the vertical direction, respectively, while the (X, Y)-plane at $Z = 0$ represents the surface into which the subsurface magnetic field emerges. R is the radius of flux tube, while L is defined as the emergence length and h is the emergence height measured from the surface, taking values between 0 and $2R$. $w \equiv 2\sqrt{(2R-h)h}$ is the emergence width. The top-left panel shows that the axis field line (thick black line) is below the surface (Phase I; $0 \le h \le R$), while it emerges above the surface at the top-right panel (Phase II; $R < h \le 2R$). Figure 1b shows a magnetic structure formed dynamically through flux emergence at Phase I (left panel) and Phase II (right panel), which is obtained from a magnetohydrodynamic (MHD) simulation for solving a forward problem of flux emergence: how the time evolution of surface magnetic field is determined when physical properties of subsurface magnetic field are assumed (Magara 2012). The aim of this paper is to use an inversion method and derive physical properties of the subsurface magnetic field from the time evolution of surface magnetic field, and compare these properties with those assumed in the simulation so as to show how well the inversion works.

Corresponding author: T. Magara

2. Evolution of Surface Magnetic Field

To represent the evolution of surface magnetic field, we focus on two quantities. One of them is emerged magnetic flux, which is classified into unsigned magnetic flux passing through the (X, Y)-plane, and signed magnetic flux passing through the (X, Z)-plane above the (X, Y)-plane. While the latter represents net emerged magnetic flux, the former counts the number of times that a single magnetic field line passes through the (X, Y)-plane, as shown by the green helices in Figure 1a. To distinguish them, the former is called apparent emerged magnetic flux $\Phi^A_{\rm emg}$ and the latter is net emerged magnetic flux $\Phi^N_{\rm emg}$. The apparent emerged

flux is solely given by the azimuthal magnetic flux of a cylindrical flux tube at Phase I:

$$\Phi^A_{\rm emg}(\text{Phase I}) = \Phi_{\rm az}(h) \tag{1}$$

where

$$\Phi_{\rm az}(h) \equiv \int_{-w/2}^{w/2} |B_Z(X,h)|\ dX \int_{-L/2}^{L/2} dY. \tag{2}$$

Here $B_Z(X,h)$ gives the distribution of azimuthal flux through the (X,Y)-plane, represented by the red-blue maps in Figure 1a. At Phase II the apparent emerged flux is obtained by adding the azimuthal flux defined by Equation (2) to the axial magnetic flux $\Phi^D_{\rm ax}$ contained in the detached portion of flux tube indicated by the yellow cylinder at the top-right panel of Figure 1a. This axial flux and the axis field line eventually pass through the (X,Y)-plane, as shown by the yellow and black dashed curves. Namely,

$$\Phi^A_{\rm emg}(\text{Phase II}) = \Phi_{\rm az}(h) + 2\ |\Phi^D_{\rm ax}(h)|, \tag{3}$$

where $\Phi^D_{\rm ax}(h)$ is the detached axial flux defined as

$$\Phi^D_{\rm ax}(h) \equiv \iint_{X^2+(Z-r_D)^2 \le {r_D}^2} B_Y(X,Z,h)\ dX\ dZ, \tag{4}$$

where $r_D = h - R > 0$ (see the bottom-right panel of Figure 1a). Here $B_Y(X,Z,h)$ gives the distribution of axial flux through the (X,Z)-plane. The factor 2 in front of the detached axial flux in Equation (3) comes from the fact that after emergence the axial field lines become curved and pass through the (X,Y)-plane at two regions indicated by the yellow dashed curves. On the other hand, the net emerged flux is always given by the axial flux above the (X,Y)-plane:

$$\Phi^N_{\rm emg}(\text{Phases I, II}) = \iint_{Z\ge 0} B_Y(X,Z,h)\ dX\ dZ. \tag{5}$$

The other quantity representing the evolution of surface magnetic field is the magnetic helicity injected across the (X,Y)-plane as flux emergence proceeds. Here we use the relative magnetic helicity introduced by Berger & Field (1984), which can be uniquely determined in a volume with magnetic flux passing through a surface surrounding that volume, while it keeps gauge invariant (Finn & Antonsen 1985). In the present model, we estimate the amount of injected magnetic helicity by calculating the relative magnetic helicity contained in the emerged portion of flux tube:

$$H_{\rm m}(\text{Phases I, II}) = \int_0^{\Phi^N_{\rm emg}} \frac{b}{2\pi^2}\ \Phi_{\rm ax}\ d\Phi_{\rm ax} \int_{-L/2}^{L/2} dY, \tag{6}$$

where $\Phi_{\rm ax}$ is the axial flux described in Priest & Forbes (2000) and $\Phi^N_{\rm emg}$ is given by Equation (5). Here $b \equiv 2\pi/l$ represents the twist of a field line making one helical turn around the axis of flux tube over the distance l. We use b as one of the parameters characterizing the subsurface magnetic field. In this case, a possible function form of subsurface magnetic field may be given by $\mathbf{B} = B_0(b_0\ r\ \hat{\theta} + \hat{z})/(1 + {b_0}^2\ r^2)$, where $\hat{z}$ and $\hat{\theta}$ determine the axial and azimuthal directions of a cylindrical flux tube, while r, B_0, and b_0 represent the radial distance from the axis of flux tube ($0 \le r \le R$), the strength of magnetic field at the axis of flux tube, and the value of uniform twist, respectively. This is the so-called Gold-Hoyle flux tube (Gold & Hoyle 1960), generating a family of flux tubes with two extremes, one of which is composed of straight field lines ($b_0 = 0$) while the other is composed of almost ring-like field lines except at the axis of flux tube ($|b_0| \to \infty$). In the present model, (R, B_0, b_0) are parameters representing physical properties of subsurface magnetic field.

Next, we consider the quantitative representation of a time-dependent process of flux emergence. In the present model, this is conducted by introducing two time-dependent functions, $h = h(t)$, $L = L(t)$, where t is time. These functions suggest that the emergence height is expressed as a function of the emergence length, $h = {\rm fef}(L)$, where fef means flux-emergence function. We use the following flux-emergence function with three characteristic parameters:

$${\rm fef}(L) = h_{\rm max}\ \sin\left[\frac{\pi}{2}\left(\frac{L}{L_{\rm max}}\right)^{\delta}\right], \tag{7}$$

where $h_{\rm max}$ and $L_{\rm max}$ are the maximum values of the emergence height and length, while $\delta > 0$ is a parameter that controls how flux emergence proceeds. Figure 2a shows three flux-emergence functions corresponding to half-emergence $(h_{\rm max}, L_{\rm max}, \delta) = (R, 15R, 1)$, intermediate-emergence $(1.5R, 15R, 2)$, and full-emergence $(2R, 15R, 0.5)$ cases, represented by black, blue and red curves, respectively. When δ takes a smaller value, flux emergence proceeds more rapidly at an early phase and then it becomes saturated, leading toward a relatively long late phase.

A set of the six parameters (R, B_0, b_0, $h_{\rm max}$, $L_{\rm max}$, δ) quantitatively characterizes the emergence of subsurface magnetic field in such a way that it determines the evolutionary path of a magnetic structure formed through flux emergence. To show this, we start by expressing the distributions of azimuthal and axial flux through the (X,Y) and (X,Z)-planes, provided by a Gold-Hoyle flux tube:

$$B_Z(X,h) = -B_0\ \frac{b_0\ X}{1 + b_0^2\ \left[X^2 + (R-h)^2\right]}, \tag{8}$$

and

$$B_Y(X,Z,h) = B_0\ \frac{1}{1 + b_0^2\ \left[X^2 + (Z-h+R)^2\right]}. \tag{9}$$

By substitute Equation (8) into Equation (2), we obtain

$$\Phi_{\rm az}(h) = \frac{B_0\ L}{|b_0|}\ \ln\left[\frac{1 + b_0^2\ R^2}{1 + b_0^2\ (R-h)^2}\right]. \tag{10}$$

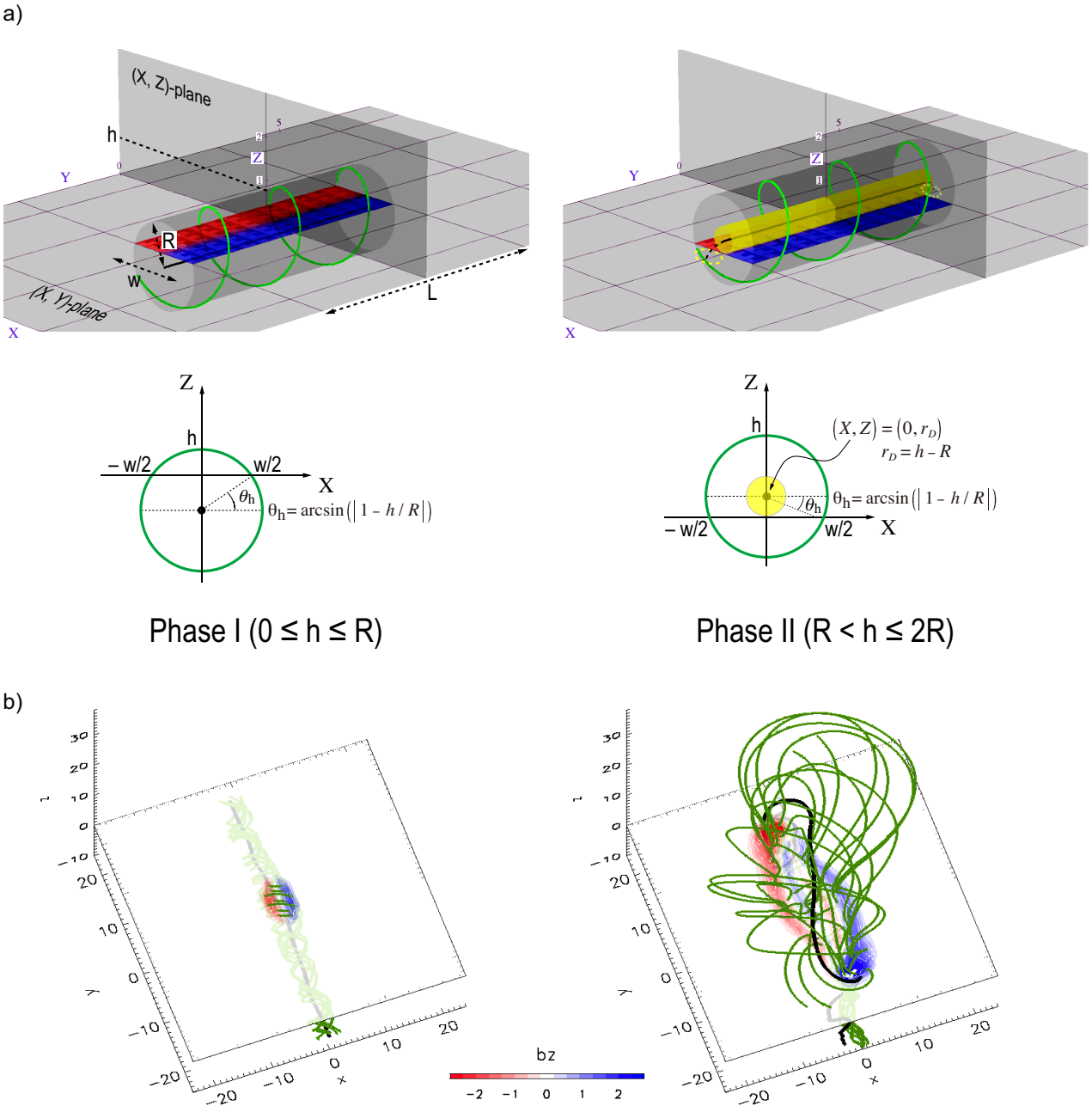

Figure 1. a): A model for the emergence of a cylindrical flux tube is schematically illustrated. At top-left panel, the axis field line of flux tube (thick black line) is below the (X, Y)-plane (Phase I), while it is above that plane at top-right panel (Phase II). At these panels, the green helix represents a helical field line surrounding the axis field line, while the blue-and-red map shows the distribution of azimuthal magnetic flux through the (X, Y)-plane. The yellow cylinder at top-right panel indicates the detached portion of flux tube, and axial magnetic flux and the axis field line contained in this portion eventually pass through the (X, Y)-plane, as shown by the yellow and black dashed curves. The cross section of flux tube in the (X, Z)-plane is presented at bottom-left and right panels. h, L, w are the emergence height, length, width, normalized by the flux-tube radius R. b): Snapshots of a magnetic structure obtained from MHD simulation of flux emergence are presented at left (Phase I) and right (Phase II) panels, where left-handed twist is initially applied to subsurface magnetic field (Magara 2012).

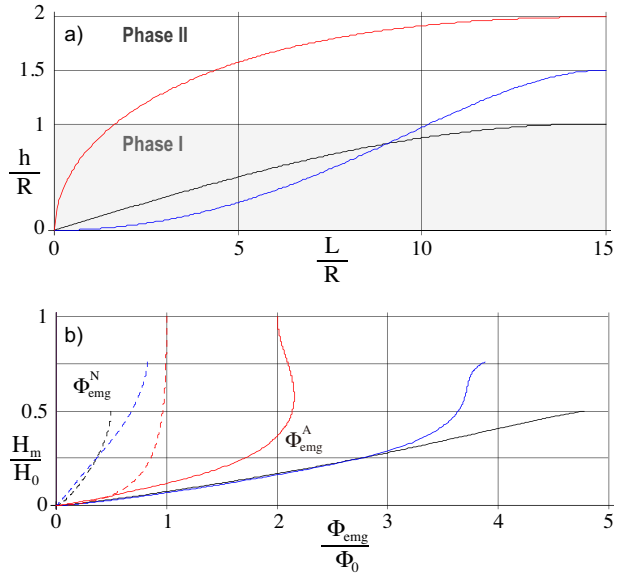

Figure 2. a): Graphs of three flux-emergence functions are drawn in black for half-emergence $(h_{\max}, L_{\max}, \delta) = (R,\ 15R,\ 1)$, blue for intermediate-emergence $(1.5R,\ 15R,\ 2)$, and red for full-emergence $(2R,\ 15R,\ 0.5)$ cases. b): Evolutionary paths based on these three flux-emergence functions are presented, showing the variation in injected magnetic helicity with apparent (solid curves) and net (dashed curves) emerged magnetic flux. $\Phi_0 = \pi B_0 b_0^{-2} \ln\left(1 + b_0^2\ R^2\right)$, $H_0 = (2\pi)^{-1} b_0\ \Phi_0^2\ L_{\max}$, and $b_0 = 1/R$.

Also, by substituting Equation (9) into Equation (4), we obtain

$$|\Phi^D_{\rm ax}(h)| = \frac{\pi\ B_0}{b_0^2}\ \ln\left[1 + b_0^2\ (R-h)^2\right]. \qquad (11)$$

The apparent emerged flux is obtained by substituting Equation (10) into Equation (1) for Phase I, and by substituting Equation (10) and Equation (11) into Equation (3) for Phase II:

$$\Phi^A_{\rm emg}(\text{Phase I}) = \frac{B_0\ L}{|b_0|}\ \ln\left[\frac{1 + b_0^2\ R^2}{1 + b_0^2\ (R-h)^2}\right], \qquad (12)$$

and

$$\Phi^A_{\rm emg}(\text{Phase II}) = \frac{B_0\ L}{|b_0|}\ \ln\left[\frac{1 + b_0^2\ R^2}{\left\{1 + b_0^2\ (R-h)^2\right\}^{1 - \frac{2\pi}{|b_0|\ L}}}\right]. \qquad (13)$$

To calculate the net emerged flux, we introduce the angle $\theta_h \equiv \arcsin\left(|1 - h/R|\right)$ which takes values between 0 and $\pi/2$, as shown by the bottom panels of Figure 1a. The net emerged flux at Phases I and II is then expressed as follows:

$$\Phi^N_{\rm emg}(\text{Phase I}) = \int_{\theta_h}^{\pi-\theta_h} d\theta \int_{\frac{R-H}{\sin\ \theta}}^{R} r\ B_z(r)\ dr, \qquad (14)$$

and

$$\Phi^N_{\rm emg}(\text{Phase II}) = \Phi_0 - \Phi^N_{\rm emg}(\text{Phase I}), \qquad (15)$$

where $B_z(r) = B_0(1 + b_0^2\ r^2)^{-1}$ and $\Phi_0 = \pi B_0 b_0^{-2} \ln\left(1 + b_0^2\ R^2\right)$ are the axial magnetic field and the total net magnetic flux of a Gold-Hoyle flux tube. By substituting these into Equation (14) and Equation (15), we obtain

$$\Phi^N_{\rm emg}(\text{Phase I}) = \frac{B_0}{2b_0^2}\times \left[(\pi - 2\theta_h)\ln\left(1 + b_0^2\ R^2\right) - \int_{\theta_h}^{\pi-\theta_h} \Theta(\theta)\ d\theta\right], \qquad (16)$$

and

$$\Phi^N_{\rm emg}(\text{Phase II}) = \frac{B_0}{2b_0^2}\times \left[(\pi + 2\theta_h)\ln\left(1 + b_0^2\ R^2\right) + \int_{\theta_h}^{\pi-\theta_h} \Theta(\theta)\ d\theta\right], \qquad (17)$$

where

$$\Theta(\theta) = \ln\left[1 + \frac{b_0^2\ (R-h)^2}{\sin^2\theta}\right]. \qquad (18)$$

Finally, by substituting Equation (16) and Equation (17) into Equation (6), we obtain the injected magnetic helicity at Phases I and II:

$$H_{\rm m}(\text{Phase I}) = \frac{B_0^2\ L}{4b_0^3}\times \left[(\pi - 2\ \theta_h)\left\{\ln\left(1 + b_0^2\ R^2\right)\right\}^2 - \int_{\theta_h}^{\pi-\theta_h} \Theta^2(\theta)\ d\theta\right], \qquad (19)$$

and

$$H_{\rm m}(\text{Phase II}) = \frac{B_0^2\ L}{4b_0^3}\times \left[(\pi + 2\ \theta_h)\left\{\ln\left(1 + b_0^2\ R^2\right)\right\}^2 + \int_{\theta_h}^{\pi-\theta_h} \Theta^2(\theta)\ d\theta\right]. \qquad (20)$$

By recalling that $h = \text{fef}(L)$, $\Phi^A_{\rm emg}$, $\Phi^N_{\rm emg}$, and $H_{\rm m}$ are expressed as functions of L, which defines a curve in $(\Phi_{\rm emg}, H_{\rm m})$-space. Since L is a variable increasing as flux emergence proceeds, the curve represents the evolutionary path of a magnetic structure formed through flux emergence. Figure 2b shows evolutionary paths based on the three flux-emergence functions presented in Figure 2a. In the full-emergence case (red curves), $\Phi^A_{\rm emg}$ is eventually equal to $2\Phi^N_{\rm emg}$ or $2\Phi_0$, because no azimuthal flux passes through the (X, Y)-plane and only the axial flux contributes to producing $\Phi^A_{\rm emg}$. In this case, $H_{\rm m}$ reaches the maximum $H_0 = (2\pi)^{-1} b_0\ \Phi_0^2\ L_{\max}$.

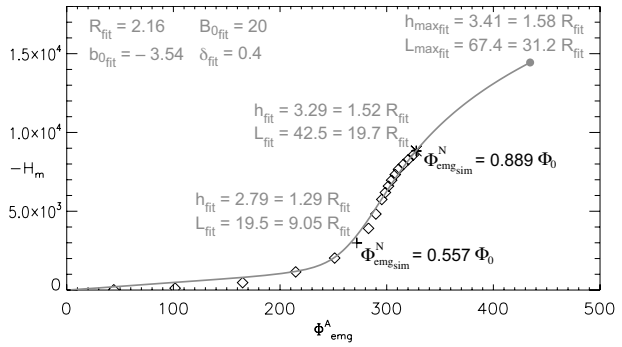

Figure 3. Data points (simulation) and a fitting curve (inversion) are presented in $(\Phi^A_{\rm emg}, H_{\rm m})$-space, which are drawn in black and gray, respectively. + and ∗ indicate a half-emergence state and the state shown by right panel of Figure 1b.

3. RESULT

Let us demonstrate the inversion process of deriving physical properties of subsurface magnetic field from an evolutionary relation between two observables, $H_{\rm m}$ and $\Phi^A_{\rm emg}$. Here we only consider the apparent emerged flux because the net emerged flux is not directly observed. Figure 3 shows data points in $(\Phi^A_{\rm emg}, H_{\rm m})$-space, which are obtained from the MHD simulation mentioned above. The first and last data points correspond to the left and right panels of Figure 1b. A curve fitting is then applied to these data points, and a best fitting curve drawn in gray gives $R_{\rm fit} = 2.16$, $B_{0\rm fit} = 20.0$, $b_{0\rm fit} = -3.54$ (left-handed twist) for the physical properties of subsurface magnetic field, and $h_{\rm max fit} = 1.58 R_{\rm fit}$, $L_{\rm max fit} = 31.2 R_{\rm fit}$, and $\delta_{\rm fit} = 0.4$ for the process of flux emergence. In the simulation, a flux tube with $R_{\rm sim} = 2$, $B_{0\rm sim} = 17.4$, $b_{0\rm sim} = -1$ is assumed as the initial state of subsurface magnetic field, so the radius and magnetic field strength are well matched with those obtained by inversion, although there is a more than 3 times difference in the value of twist. A possible explanation of this discrepancy is that after they emerge, magnetic field lines tend to be twisted strongly around the footpoints of the axis field line (Magara 2004), which may enhance the inversion value compared to the value of uniform twist initially assumed in the simulation. As for the process of flux emergence, the right panel of Fig. 1b shows that the emergence length is observed as $L_{\rm sim} \sim 36 = 18 R_{\rm sim}$, while the fitting curve gives $L_{\rm fit} = 42.5 = 19.7 R_{\rm fit}$ at the corresponding data point. The emergence height at this data point is $h_{\rm fit} = {\rm fef}(42.5) = 3.29 = 1.52 R_{\rm fit}$, suggesting that intermediate-emergence proceeds, which is observed at the right panel of Figure 1b. Furthermore, the fitting curve specifies a half-emergence state indicated by a plus in Figure 3. This shows that the inversion seems to work well for the process of flux emergence.

4. DISCUSSION

It is well known that the Sun shows periodic variation of magnetic activity, producing solar activity cycles represented historically by the number of sunspots observed at the base of solar active regions (Schwabe 1844). For understanding the mechanism of solar activity cycles, physical properties of the magnetic field forming sunspots are important (Choudfuri et al. 2007). Determining evolutionary paths of active regions in $(\Phi^A_{\rm emg}, H_{\rm m})$-space is a key to these properties, as demonstrated above. This requires continuous observations of photospheric vector magnetic field from the birth to a developed state of each active region, combined with the method for deriving injected magnetic helicity from observed data (Chae 2001; Kusano et al. 2002; Démoulin & Berger 2003; Magara & Tsuneta 2008). In fact, long-term temporal development of $H_{\rm m}$ and $\Phi^A_{\rm emg}$ has been derived from observed data in several active regions (Jeong & Chae 2007). When this kind of work will be performed for the period of a solar activity cycle, the inversion method presented here may provide the physical properties of subsurface magnetic field responsible for solar magnetism. Toward this end, we will investigate the applicability of this method to observed data in our succeeding paper.

ACKNOWLEDGMENTS

The author deeply appreciates productive comments given by the referee. He also wishes to thank the Kyung Hee University for general support of this work. This work was financially supported by Core Research Program (NRF-2017R1A2B4002383, PI: T. Magara) through the National Research Foundation of Korea (NRF) funded by the Ministry of Education, Science and Technology, as well as by BK21 plus program through the NRF.

REFERENCES

Berger, M. A., & Field, G. B. 1984, The Topological Properties of Magnetic Helicity, Journal of Fluid Mechanics, 147, 133

Chae, J. 2001, Observational Determination of the Rate of Magnetic Helicity Transport through the Solar Surface via the Horizontal Motion of Field Line Footpoints, ApJ, 560, L95

Choudhuri, A. R., Chatterjee, P., & Jiang, J. 2007, Predicting Solar Cycle 24 With a Solar Dynamo Model, Physical Review Letters, 98, 131103

Démoulin, P., & Berger, M. A. 2003, Magnetic Energy and Helicity Fluxes at the Photospheric Level, Solar Physics, 215, 203

Fan, Y. 2009, Magnetic Fields in the Solar Convection Zone, Living Reviews in Solar Physics, 6, 4

Finn, J. M., & Antonsen, T. M. 1985, Magnetic Helicity: What Is It, and What Is It Good for?, Comments Plasma Phys. Controlled Fusion, 26, 111

Gold, T., & Hoyle, F. 1960, On the Origin of Solar Flares, MNRAS, 120, 89

Jeong, H., & Chae, J. 2007, Magnetic Helicity Injection in Active Regions, ApJ, 671, 1022

Kliem, B., & Török, T. 2006, Torus Instability, Physical Review Letters, 96, 255002

Kusano, K., Maeshiro, T., Yokoyama, T., & Sakurai, T. 2002, Measurement of Magnetic Helicity Injection and Free Energy Loading into the Solar Corona, ApJ, 577, 501

Low, B. C. 1996, Solar Activity and the Corona, Solar Physics, 167, 217

Magara, T. 2004, Injection of Magnetic Energy and Magnetic Helicity into the Solar Atmosphere by an Emerging Magnetic Flux Tube, The Solar-B Mission and the Forefront of Solar Physics, ASPC, 325, 185

Magara, T., & Tsuneta, S. 2008, Hinode's Observational Result on the Saturation of Magnetic Helicity Injected into the Solar Atmosphere and Its Relation to the Occurrence of a Solar Flare, Publication of Astronomical Society of Japan, 60, 1181

Magara, T. 2012, How Much Does a Magnetic Flux Tube Emerge into the Solar Atmosphere?, ApJ, 748, 53

Moreno-Insertis, F., & Emonet, T. 1996, The Rise of Twisted Magnetic Tubes in a Stratified Medium, ApJ, 472, L53

Parker, E. N. 1955, The Formation of Sunspots from the Solar Toroidal Field, ApJ, 121, 491

Priest, E. R., & Forbes, T. G. 2000, Magnetic Reconnection: MHD Theory and Applications (Cambridge: Cambridge University Press), 268

Priest, E. R., & Forbes, T. G. 2002, The Magnetic Nature of Solar Flares, A&SR, 10, 313

Schwabe, M. 1844, Sonnenbeobachtungen im Jahre 1843. Von Herrn Hofrath Schwabe in Dessau, Astronomische Nachrichten, 21, 233

Shibata, K., & Magara, T. 2011, Solar Flares: Magnetohydrodynamic Processes, Living Reviews in Solar Physics, 8, 6